Journal of Computational Physics **171,** 579–615 (2001)
doi:10.1006/jcph.2001.6797, available online at http://www.idealibrary.com on IDEAL®

Transmission of a Slowly Moving Shock across a Nonconservative Interface[1]

Zi-Niu Wu

Department of Engineering Mechanics, Tsinghua University, Beijing 100084, P.R. China
E-mail: ziniuwu@tsinghua.edu.cn

Received March 15, 2000; revised December 15, 2000

Computational fluid dynamics using composite overlapping grids plays an important role in today's fluid mechanics with complex flows. The key point in the overlapping grid method is how to ensure conservation for shock waves. This was first studied by M. Berger under the framework of weak solutions for vanishing mesh size, leading to the well-known flux interpolation interface condition (*SIAM J. Numer. Anal.* **24**, 967(1987)). The present author used the Rankine–Hugoniot relation to directly analyze the transmission of a shock across the interface and showed that, for the scalar Burgers equation, a nonconservative treatment leads to correct transmission of shocks even for finite mesh sizes if the interior difference scheme contains enough dissipation, and that shock penetration trouble only occurs for very slowly moving shock waves (*SIAM J. Sci. Comput.* **20**, 1850 (1999)). This is reconsidered here for the system of Euler equations in gas dynamics. Numerical experiments show that for weakly dissipative schemes, slowly moving shock waves fail to transmit the nonconservative interface by producing finally a nonphysical, two-shocked steady-state solution. By using the dynamics of a very slowly moving shock, we will show that two-shocked steady-state solutions are avoided if the interior difference scheme is no less dissipative than the standard Roe scheme even though a nonconservative interface treatment is used.

Key Words: slowly moving shock; shock/interface transmission; two-shocked solution; nonconservative grid interface.

1. INTRODUCTION

Flows around multielement bodies can be efficiently analyzed by computational fluid dynamics using composite overlapping grids. If a moving shock fails to transmit the grid interface, then the solution has no meaning. A correct prediction of the shock speed or

[1] This work was supported by Chinese National Natural Science Foundation under Contract Number 10025210.

0021-9991/01 $35.00

position is very important since it determines the lift force and sometimes the main part of drag force for transonic and supersonic airfoils. The possible trouble of shock/interface transmission can be understood from a mechanical point of view. In fact, a moving shock itself has some energy. When the shock impinges the grid interface, some energy would get lost due to the interface. Thus it can be readily imagined that a very slowly moving shock would possibly have some difficulty in transmitting the interface since the energy involved in the shock should be proportional to the shock speed. The possible blocking of the shock wave can be also understood in a mathematical way, by noting that the discrete Euler equations in gas dynamics on overlapping grids are equivalent to the so-called modified equations [11], which are just the Euler equations plus some source terms. The source terms become important at the grid interfaces [24]. Generally, the source terms can be divided into three parts:

(a) Zeroth-order terms: The case of a hyperbolic system with moving source term has been analyzed by Lin who shows that nonlinear resonance may occur in such a case [19]. Such zeroth-order terms may be a cause of shock blocking.

(b) Dissipative terms (with space derivatives of even order): The role of dissipation is similar to the viscous force of a viscous fluid; namely, it just smooths out the sharp shock wave.

(c) Dispersive terms (with space derivatives of odd order): The interaction between a shock and a dispersive wave would lead to the change of shock speeds [4]. This is another cause of shock blocking.

The difficulty of slowly moving shock waves exists also for numerical treatments without interfaces [2, 3, 12, 15, 18, 20, 21, 27, 39].

The only difference between the overlapping grid method and a single domain treatment is that the former requires interpolation at the grid interfaces. Conventional interpolation, or normal interpolation, is based on the state variables. Since the interpolation is performed inside the grid, the local conservation of the difference approximation is altered. When the solution is smooth or just contains contact discontinuities, the loss of conservation is unimportant. However, when shock waves interact with the grid interface, conservation would be required according to the general theory of weak solution. Based on earlier numerical remarks on the importance of conservation, Berger [5] constructed interface treatment based on flux interpolation which ensures conservation in the weak sense. This is a very important achievement followed by many subsequent studies [7, 24, 25, 31, 34]. The normal interpolation, which does not fulfill the conservation requirement, is simpler and more stable than the flux interpolation method. But is it necessary to have conservative treatment for conservative solutions?

For multimaterial interfaces, Karni [13] was able to obtain conservative results with nonconservative treatment. The method proposed by Karni [13] is nonconservative on the entire domain and could not handle strong shocks as was pointed out by Abgrall [1]. This was remedied in [9, 14] in which the methods are nonconservative only on a lower dimensional set near the interface. Tang and Zhou [31] examined the conservation error of nonconservative overlapping grid treatment still under the framework of weak solutions for vanishing mesh size.

Any real computation is done on a grid with finite mesh sizes. Thus it appears more useful to examine conservation on a grid with finite mesh sizes. This is the approach adopted by the present author [36]. Since conservation is important only for genuinely nonlinear discontinuous waves, the real key point of conservation is whether a moving

shock can transmit the overlapping grid interface without difficulty. Let us state the argument more clearly. Imagine two partially overlapping grids in 1D, with possibly different mesh spacing. Interpolation procedures are needed in order to orchestrate the solutions on both sides. A shock wave approaching the overlapping region needs to continue its motion from one grid into the next, ideally, without noticing the grid change. Less ideally, the interpolation procedures may be such that will cause a delay in shock transmission, which is still OK if the error (delay) goes to zero with mesh refinement. What is not OK is if the shock gets stuck at the edge of the grid interface and stays there forever, thus causing nonconvergence of the solution. Nonconservative interpolation procedures may trigger such behavior. By considering the direct interaction between a right-going shock of the Burgers equation and an overlapping grid interface, the present author has obtained the following results:

(a) if the interface treatment is defined by Berger's flux interpolation, then the shock can transmit the grid interface without delay. This had already been proved by Berger [5] using the argument of convergence to weak solutions for vanishing mesh size. But the analysis in [36] is for finite mesh size and this conclusion remains valid for a system of equations.

(b) if the physical shock speed normalized by the wave speed in the left of the shock is larger than $s_{\min} = \frac{1}{2} - \frac{\sqrt{2}}{4} \approx 0.146$ and smaller than $s_{\max} = \frac{1}{2} + \frac{\sqrt{2}}{4} \approx 0.854$, then the numerical shock can transmit the grid interface even with nonconservative normal interpolation. This is just a sufficient condition that was derived rigorously by analysis. For a specific scheme, the lower bound $s_{\min}$ can be reduced, and the upper bound $s_{\max}$ can be increased. There is no difficulty in understanding the lower bound as already explained in the Introduction. The upper bound only possibly exists for numerical schemes with strong numerical oscillations near shock waves. It is very rare to use a strongly oscillatory scheme to compute shock flows in practice. Hence only slowly moving shock waves could have trouble. For slowly moving shock waves, it is necessary that one eigenvalue changes sign across the shock layer (e.g., [15], see also Sect. 3.4 of [36], where it was shown that for a shock speed smaller than $s_{\min}$, one eigenvalue changes sign).

(c) if the numerical viscosity of the interior difference equations, just at the interface point and at the moment that the shock coincides with the interface, is no smaller than that of the standard first-order Roe scheme, then the numerical shock can transmit the grid interface even with nonconservative normal interpolations and for all shock speeds.

(d) the numerical shock fails to transmit the grid interface only if the shock speed is very slow, the interpolation is nonconservative, and the interior difference scheme does not have enough dissipation.

The sufficient conditions a–c are obtained theoretically, and the necessary condition d is based on numerical experiments. These results show that the range in which an overlapping grid method fails to work is very narrow. In fact, modern schemes for shock flow computation have enough numerical dissipation inside the shock so that sufficient condition c is satisfied. However, the above results are basically based on the scalar Burgers equation, though some numerical experiments given in [36] seem to justify that they remain true even for the Euler equations in gas dynamics.

The purpose of this study is to extend part of the scalar results to the system of Euler equations in gas dynamics. For slowly moving shock waves, we observe numerically that the shock fails to transmit the interface by producing a nonphysical, two-shocked steady state if the numerical scheme is weakly dissipative and if the interface treatment is nonconservative.

However, if the interior difference equations contain enough numerical dissipation, the two-shocked steady-state solutions are avoided even if we use nonconservative normal interface interpolation. The theoretical proof relies heavily on the dynamics of a slowly moving shock wave. We are actually unable to do so for a general hyperbolic system of equations.

This paper will be organized as follows.

In Section 2, the basic condition of shock/interface transmission is derived for a general hyperbolic system approximated by conservative schemes and for an interface condition defined by nonconservative normal interpolation. It is the condition of a two-shocked steady state that is stated. Actually we find that if the condition of a two-shocked solution does not hold, then the shock can transmit the grid interface.

In Section 3 we prove that a slowly moving shock for the Euler equations in gas dynamics cannot stick to the interface in the form of two-shocked steady state, if the interior difference contains no less dissipation than the standard Roe scheme, just at the point of shock/interface interaction.

In Section 4 we provide some discussion and numerical experiments. Concluding remarks will be given in Section 5.

2. BASIC CONDITION OF SHOCK/INTERFACE TRANSMISSION

2.1. *Difference Approximations on Overlapping Grids*

Consider the following hyperbolic system of conservation laws

$$W_t + H_x = 0, \quad t \in \mathbb{R}^+, \quad x \in \mathbb{R}, \tag{1}$$

where the unknown W is called the state variable or conservative variable, and $H = H(W)$ is called the flux function.

Similarly as in [36], the computational domain is split into two subdomains $D_u = \{x\colon x < b\}$, $D_v = \{x\colon -a < x\}$ with an overlapping length $b + a$. The boundaries $x = -a$ and $x = b$ of the overlap are called interfaces. The overlap $(-a, b)$ contains p points in the right subdomain and q points in the left subdomain.

The numerical solutions in D_u and D_v are denoted as $U_j^n \approx W(x_j^{(u)}, n\delta t)$ with $j \le 0$ and $V_j^n \approx W(x_j^{(v)}, n\delta t)$ with $j \ge 0$, where $x_j^{(u)} = b + (j - 0.5)\delta x_u, x_j^{(v)} = -a + (j + 0.5)\delta x_v$ are cell centers, and δt, δx_u, and δx_v define respectively the time step, the mesh size in D_u, and the mesh size in D_v. The ratios $\sigma_u = \delta t/\delta x_u$, $\sigma_v = \delta t/\delta x_v$ are assumed to be constant. In each subdomain, the system (1) is approximated by a multilevel and $(l + r + 1)$-point difference scheme in conservation form:

$$\Delta V_j^n = -\sigma_u\big(F_{j+1/2}^n - F_{j-1/2}^n\big), \quad \Delta V_j^n = -\sigma_v\big(G_{j+1/2}^n - G_{j-1/2}^n\big). \tag{2}$$

Here $\Delta U_j^n = U_j^n - U_j^n$ and $\Delta V_j^n = V_j^n - V_j^n$ denote the time increments, and $F_{j+1/2}^n$ and $G_{j+1/2}^n$ are numerical fluxes consistent with the exact flux function $H(W)$. For a two-level $(l + r + 1)$-point scheme, we have

$$F_{j+1/2}^n = F_{j+1/2}^n\big(U_{j-l+1}^n, U_{j-l+2}^n, \ldots, U_{j+r}^n; U_{j-l+1}^{n+1}, U_{j-l+2}^{n+1}, \ldots, U_{j+r}^{n+1}; \sigma_u\big)$$
$$G_{j+1/2}^n = G_{j+1/2}^n\big(V_{j-l+1}^n, V_{j-l+2}^n, \ldots, V_{j+r}^n; V_{j-l+1}^{n+1}, V_{j-l+2}^{n+1}, \ldots, V_{j+r}^{n+1}; \sigma_v\big),$$

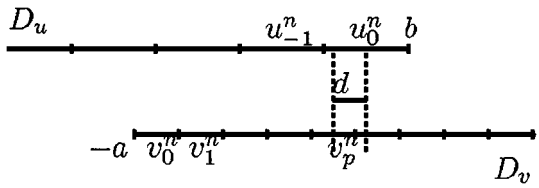

FIG. 1. Overlapping grid for normal interpolation.

with

$$F^n_{j+1/2}(U, U, \ldots, U; U, U, \ldots, U; \sigma_u) = H(U)$$
$$G^n_{j+1/2}(V, V, \ldots, V; V, V, \ldots, V; \sigma_v) = H(V).$$

It is well known [17] that the solution of a conservative scheme converges to a weak solution of the exact equation when it converges.

There are two classes of interface condition: the nonconservative normal interpolation and the conservative flux interpolation. For schemes with more than three points in space, the same interface condition can be applied to all interface points $j = 0, 1, \ldots, r-1$ for the left subdomain and $j = 0, -1, \ldots, -l+1$ for the right subdomain. This will be called *translatory interface condition*.

Let $I(x, \phi)$ be an interpolation to x using discrete values of ϕ near x.

Referring to Fig. 1, the normal interpolation, which is frequently used in practice, is based on the unknowns U^n_j and V^n_j and has the general form

$$U^n_\mu = I\left(b - \frac{1-\mu}{2}\delta x_u; V^n\right), \quad \mu = 0, 1, \ldots, r-1 \tag{3}$$

$$V^n_\mu = I\left(-a + \frac{\mu+1}{2}\delta x_v; U^n\right), \quad \mu = 0, -1, \ldots, -l+1. \tag{4}$$

See [6, 25] for more details.

In the conservative flux interpolation method [5], the values U^n_0 and V^n_0 are calculated as in the interior points, the missed numerical fluxes $F^n_{1/2}$ and $G^n_{-1/2}$ are interpolated from the interior points (see Fig. 2):

$$F^n_{1/2} = I(b; G^n), \quad G^n_{-1/2} = I(-a; F^n). \tag{5}$$

The interpolation coefficient β is similarly defined. When computing the numerical fluxes for points near the interface, we still require the values u^n_μ with $\mu = 1, 2, \ldots, r-1$ and v^n_μ

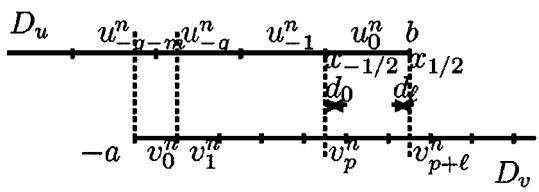

FIG. 2. Overlapping grid for flux interpolation.

with $\mu = -1, -2, \ldots, -l+1$. This can be defined by just using the normal interpolation

$$U_\mu^n = I\left(b - \frac{1-\mu}{2}\delta x_u; V^n\right), \quad \mu = 1, 2, \ldots, r-1 \tag{6}$$

$$V_\mu^n = I\left(-a + \frac{\mu+1}{2}\delta x_v; U^n\right), \quad \mu = -1, -2, \ldots, -l+1. \tag{7}$$

The interface conditions (5)–(7) combines the flux interpolation and the normal interpolation. Note that in two or three dimensions, it is not enough just to interpolate the fluxes if one wants a conservative scheme. See [5, 7].

There were quite a number of studies with regard to the accuracy [6, 26], stability [10, 22, 24, 25, 29, 32], conservation [5, 7, 25, 33], solution uniqueness [34], and convergence to a steady state [35, 37] of the overlapping grid interface treatment.

2.2. *Possible Scenarios of a Right-Going Numerical Shock*

For completeness of the presentation, let us first consider the scenario already stated in [36] for a scalar equation. Consider a single right-going shock starting in the left subdomain away from the interface. After the shock inside the left subdomain (Shock L) reaches $x = -a$, another one (Shock R) forms inside the right subdomain due to interpolation at $x = -a$. Being free of interface before reaching $x = b$, Shock L moves to the right, while Shock R may get stuck at $x = -a$ or successfully penetrates the interface. If Shock R gets stuck at $x = -a$, Shock L cannot disappear due to interpolation at $x = b$. Only inside the overlap both shocks can exist simultaneously. Ideally, we desire Shock L and Shock R to have the same position, when they are inside the overlap. Practically, we would have the following three scenarios:

Case a (perfect transmission, Fig. 3): Shock R moves at the same speed (within the difference of the order of truncation error) as Shock L. When both shocks arrive at the right boundary of the overlap ($x = b$), shock R will pass freely since it faces no boundary. When shock R moves to the right of the overlap, the solution near $x = b$ in the right subdomain becomes smooth and by interpolation shock L disappears.

Case b (delayed transmission, Fig. 4): Shock R gets stuck for a finite time interval at the left boundary of the overlap due to conservation error, while Shock L moves freely rightward until it reaches the right boundary of the overlap. Shock R starts to move late and lags a distance with respect to Shock L. When Shock L reaches the right boundary of the overlap, it stays there motionless due to interpolation and disappears after Shock R moves to the right of the overlap. Thus the right-going shock will finally transmit the overlap but with a delay with respect to the exact shock.

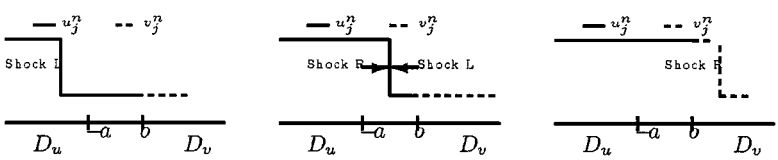

FIG. 3. Shock through the overlap in case of perfect transmission. Left: shock at the left of the overlap. Middle: shock inside the overlap. Right: shock after transmission.

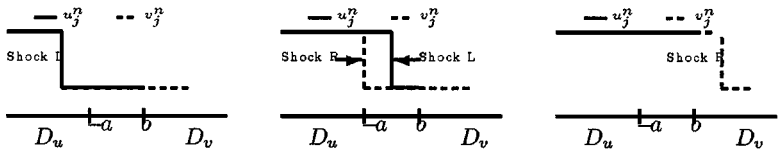

FIG. 4. Shock through the overlap in case of delayed transmission. Left: shock at the left of the overlap. Middle: shock inside the overlap. Right: shock after transmission.

Case c (no transmission, Fig. 5): Shock R always gets stuck at the left boundary of the overlap due to severe conservation error. When Shock L reaches the right boundary of the overlap, it stays there permanently due to interpolation. This leads to a two-shocked steady-state solution.

One would also imagine other scenarios. For instance, one would imagine that Shock L lags behind Shock R. This is in fact impossible since only Shock R faces an interface before both shocks arrive at $x = b$. A second possibility one would imagine is that for system of equations only part of the waves get transmitted, part get stuck, and part get reflected. However, since the interpolation normally used is done in the same way for each component of the state variables, each component should behave similarly so that the wave travels in whole and no part of the wave is preferred. As a result, the situation of partial transmission,partial sticking, and partial reflection does not appear to happen.

Perfect transmission is the most desired scenario. To see whether the delayed transmission is acceptable, let us consider the difference approximation for the Euler equations. A nondimensional analysis shows that the solution depends only on the Mach number M and the Courant number $CFL = \sigma \max(\lambda)$, where $\max(\lambda)$ denotes the maximum wave speed. Thus the delay N, in terms of number of time iterations, should be only a function of M and CFL. The specific form of this function depends on the structure of the numerical approximation. Thus the delay in terms of the dimensional time is $T = N\delta t$. By refining the mesh or equivalently the time step ($\delta t \to 0$) while keeping CFL fixed as is common in CFD, the delay T can be made as small as we desire. Thus a delayed transmission is acceptable since from the dimensional argument it can be made as small as one desires through mesh refinement.

Only the case of no transmission is unacceptable since the solution is even qualitatively altered: an unsteady shock is transformed into a nonphysical steady-state shock.

2.3. *Condition for the Existence of Nonphysical, Two-Shocked Steady-State Solution*

The two-shocked steady-state solution cannot appear arbitrarily. It must satisfy a certain number of constraints, called *condition of two-shocked solution*. Let us derive the condition of two-shocked solution.

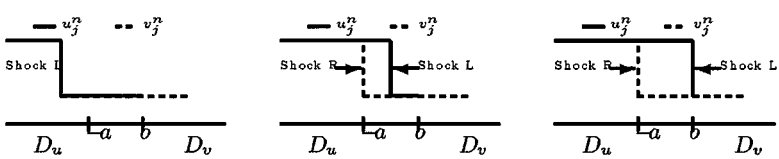

FIG. 5. Shock through the overlap in case of no transmission. Left: shock at the left of the overlap. Middle: shock inside the overlap. Right: steady-state two-shocked solution after a long time.

Once a steady-state is reached, we have $\Delta U_j^n = 0$ and $\Delta V_j^n = 0$. Thus by (2) the numerical fluxes satisfy the following conditions

$$F_{j+1/2} = F_{-\infty+1/2} \quad \forall j < 0$$
$$G_{j+1/2} = G_{\infty+1/2} \quad \forall j > 0.$$

The solutions at infinity[2] are assumed to be smooth, and by consistent assumption, we must have $F_{-\infty+1/2} = H_L$ and $G_{-\infty+1/2} = H_R$. As a result, we have the following constraint on the numerical flux

$$\begin{cases} F_{-1/2} = H_L \\ G_{1/2} = H_R. \end{cases} \tag{8}$$

Now we want to express the condition (8) in terms of the numerical viscosity of the difference equations. Let us just concentrate on $G_{j+1/2}^n$.

First consider a scalar equation, it is well known [30] that any multipoint conservative scheme can be put into a viscous form similar to a three-point scheme. In terms of the numerical flux $G_{j+1/2}^n$, the viscous form for a scalar problem can be written as

$$G_{j+1/2}^n = \frac{1}{2}\left(H_j^n + H_{j+1}^n\right) + \frac{1}{2} Q_{j+1/2}^n \left(V_j^n - V_{j+1}^n\right), \tag{9}$$

where $Q_{j+1/2}^n$ is the numerical viscosity defined by

$$Q_{j+1/2}^n = \begin{cases} \left[G_{j+1/2}^n - \frac{1}{2}\left(H_j^n + H_{j+1}^n\right)\right] \Big/ \left[\frac{1}{2}\left(V_j^n - V_{j+1}^n\right)\right], & \text{for } V_j^n \neq V_{j+1}^n \\ <\infty, & \text{for } V_j^n = V_{j+1}^n. \end{cases}$$

The influence of the extra points outside that of a three-point scheme was factored into the numerical viscosity $Q_{j+1/2}^n$.

We are wondering if it is possible to define a matrix $Q_{j+1/2}^n$ such that $G_{j+1/2}^n$ can be related to $Q_{j+1/2}^n$ by (9) in the case of a system.

PROPOSITION 1. *For the case of multipoint difference approximation, it is always possible to have a matrix numerical viscosity $Q_{j+1/2}^n$ such that* (9) *holds. This numerical viscosity is uniquely defined for the case of a scalar equation, and there is an infinite number of $Q_{j+1/2}^n$ for the case of a system.*

Proof. Let X and Y be two independent vectors each with m components; then, obviously, there exists at least one $m \times m$ matrix M such that the following relation holds

$$Y = MX.$$

In fact, the above equation has m^2 unknowns and only m relations. Hence the problem is underdetermined and has an infinite number of solutions (in the case of a scalar equation, only one solution exists).

Thus by taking $Y = G_{j+1/2}^n - \frac{1}{2}(H_j^n + H_{j+1}^n)$ and $X = \frac{1}{2}(V_j^n - V_{j+1}^n)$, we conclude that there always exists some matrix $Q_{j+1/2}^n (= M)$ such that (9) holds in the case of a system with multipoint difference approximation. ■

[2] Here the word "infinity" means sufficiently far away from the interface.

Remark 2.1. The numerical viscosity $Q^n_{j+1/2}$ satisfying (9) is nonunique. But in Section 3 we will construct a unique and more convenient viscosity to proceed with the analysis. See Proposition 2.

For convenience, let us introduce the Roe matrix [28] $\bar{C}_{j+1/2}$ defined as

$$H^n_{j+1} - H^n_j = \bar{C}_{j+1/2}\big(V^n_{j+1} - V^n_j\big) \quad \text{if } V^n_{j+1} \neq V^n_j$$
$$\bar{C}_{j+1/2} = C(V) \quad \text{if } V^n_{j+1} = V^n_j = V.$$

In terms of the numerical viscosity, the second condition in (8) can be expressed as

$$\frac{1}{2}(H_0 + H_1) + \frac{1}{2}Q_{1/2}(V_0 - V_1) = H_R. \tag{10}$$

Now let us consider the constraint due to interpolation. For the two-shocked steady-state solution, the solution is smooth inside each subdomain. The solution in the left subdomain is close to W_L and the solution in the right subdomain is close to W_R. Thus, the interface condition (6)–(7), which is assumed to be at least locally first-order accurate, reduces to

$$U_\mu = I\left(b - \frac{1-\mu}{2}\delta x_u; V\right) = W_R + E^u_\mu, \quad \mu = 1, 2, \ldots, r-1 \tag{11}$$

$$V_\mu = I\left(-a + \frac{\mu+1}{2}\delta x_v; U\right) = W_L + E^v_\mu, \quad \mu = -1, -2, \ldots, -l+1. \tag{12}$$

Here E^u_μ and E^v_μ are numerical errors due to shock smearing and oscillation. The errors E^u_μ and E^v_μ vanish when the overlap is large enough in comparison with the width of the numerical shock. Later on we will assume the overlap to be sufficiently large to have $E^u_\mu = 0$ and $E^v_\mu = 0$, so that we have from (12) the following condition

$$V_0 = W_L. \tag{13}$$

Combining (10) and (13), and making use of the relations $H_0 = H(V_0) = H(W_L) = H_L$, we have

$$\frac{1}{2}Q_{1/2}(V_0 - V_1) = (H_R - H_L) + \frac{1}{2}(H_0 - H_1),$$

which, by the Rankine–Hugoniot relation (18) and by the definition of the Roe matrix, can be rewritten as

$$\frac{1}{2}Q_{1/2}(V_0 - V_1) = s(W_R - W_L) + \frac{1}{2}\bar{C}_{1/2}(V_0 - V_1)$$

or more conveniently

$$\frac{1}{2}\big(Q_{1/2} - \bar{C}_{1/2}\big)(W_L - V_1) = s(W_R - W_L) \tag{14}$$

in which we have used $V_0 = W_L$.

Equation (14) is the final form of the condition of two-shocked solution. If the numerical viscosity $Q_{j+1/2}$ or the exact shock speed s is such that (14) cannot hold, then the shock can transmit the interface.

3. SHOCK/INTERFACE TRANSMISSION FOR THE EULER EQUATIONS IN GAS DYNAMICS

3.1. *Dynamics of a Slowly Moving Shock*

For the Euler equations in gas dynamics, the unknown W and the flux function $H = H(W)$ in (1) are defined by

$$W = \begin{pmatrix} \rho \\ \rho u \\ \rho E \end{pmatrix}, \quad H(W) = \begin{pmatrix} \rho u \\ \rho u^2 + P \\ \rho u\left(E + \frac{P}{\rho}\right) \end{pmatrix}.$$

Here ρ denotes the density, u denotes the velocity, E denotes the total energy, and P is the pressure. For a perfect gas, the pressure is related to other variables through the state equation $P = (\gamma - 1)\rho(E - \frac{1}{2}u^2)$, where γ with $\gamma > 1$ is the ratio between the specific heats at constant pressure and volume. The corresponding Jacobian matrix $C(W) = \frac{dH(W)}{dW}$ is given by

$$C(W) = \begin{pmatrix} 0 & 1 & 0 \\ \frac{\gamma-3}{2}u^2 & (3-\gamma)u & \gamma - 1 \\ (\gamma-1)u^3 - \gamma u E & \gamma E - \frac{3(\gamma-1)}{2}u^2 & \gamma u \end{pmatrix}$$

or in terms of u, $\Theta = E + P/\rho$ (total enthalpy) and $a = \sqrt{\gamma P/\rho}$(sound speed)

$$C(W) = \begin{pmatrix} 0 & 1 & 0 \\ \frac{\gamma-3}{2}u^2 & (3-\gamma)u & \gamma - 1 \\ (\gamma-1)u^3 - \gamma u\Theta + ua^2 & \gamma\Theta - a^2 - \frac{3(\gamma-1)}{2}u^2 & \gamma u \end{pmatrix}.$$

The eigenvalues of this Jacobian matrix are $\lambda_1 = u$, $\lambda_2 = u + a$, $\lambda_3 = u - a$. Let

$$\Lambda = \begin{pmatrix} u & 0 & 0 \\ 0 & u + a & 0 \\ 0 & 0 & u - a \end{pmatrix}.$$

Then the diagonalization matrices of $C(W)$, i.e., the matrices L^{-1} and L which ensure the relation $L^{-1}\,C(W)L = \Lambda$, are given by

$$L^{-1} = \begin{pmatrix} 1 - \frac{1}{2a^2}(\gamma-1)u^2 & -\frac{1}{a^2}(1-\gamma)u & -\frac{1}{a^2}(\gamma-1) \\ -u + \frac{1}{2a}(\gamma-1)u^2 & 1 + \frac{1}{a}(1-\gamma)u & \frac{1}{a}(\gamma-1) \\ -u - \frac{1}{2a}(\gamma-1)u^2 & 1 - \frac{1}{a}(1-\gamma)u & -\frac{1}{a}(\gamma-1) \end{pmatrix} \tag{15}$$

$$L = \begin{pmatrix} 1 & \frac{1}{2}\frac{1}{a} & -\frac{1}{2}\frac{1}{a} \\ u & \frac{1}{2}\left(1 + \frac{u}{a}\right) & \frac{1}{2}\left(1 - \frac{u}{a}\right) \\ \frac{1}{2}u^2 & \frac{1}{4}u^2\frac{1}{a} + \frac{1}{2}u + \frac{1}{2(\gamma-1)}a & -\frac{1}{4}u^2\frac{1}{a} + \frac{1}{2}u - \frac{1}{2(\gamma-1)}a \end{pmatrix}. \tag{16}$$

Consider a right-going shock with the following initial data

$$W(x,0) = W_L, \quad x < x_0; \qquad W(x,0) = W_R, \quad x > x_0 \tag{17}$$

which satisfy the Rankine–Hugoniot jump relation

$$H_R - H_L = s'(W_R - W_L). \tag{18}$$

Here $x_0 < -a$, s' is the shock speed, and $H_L = H(W_L)$, $H_R = H(W_R)$.

We will just consider a right-going shock with $s' > 0$. The case of a left-going shock can be analyzed in a similar way and the conclusion remains the same. Besides, we only consider the case with $u_L > 0$.

Now let us state some important properties of the jump in conservative variables. The details for the derivation of these properties are ignored here and will be published in [38] where we will also treat the problem of momentum spike and post-shock oscillation.

Let $\bar{M}_L$ be the relative Mach number in the left-hand side of the shock defined by

$$\bar{M}_L = \frac{u_L - s'}{\sqrt{\gamma \frac{P_L}{\rho_L}}} = M - \frac{s'}{\sqrt{\gamma \frac{P_L}{\rho_L}}}.$$

Here $M = u_L / \sqrt{\gamma \frac{P_L}{\rho_L}}$ is the Mach number in the left-hand side of the shock.

For convenience, let us take $\rho_L = P_L = 1$ and $u_L = \sqrt{\gamma} M$. This is not a restriction by nondimensional treatment. The shock speed relative to the sound speed $a_L = \sqrt{\gamma \frac{P_L}{\rho_L}} = \sqrt{\gamma}$ is defined by $s = \frac{s'}{a_L}$. Only the relative shock speed will be used.

For a prescribed shock speed s, the jump of conservative variables in terms of M and s is found to be

$$\rho_R - \rho_L = \frac{(\gamma+1)\gamma(M-s)^2}{(\gamma-1)\gamma(M-s)^2 + 2\gamma} - 1 \tag{19}$$

$$\rho_R u_R - \rho_L u_L = \frac{(\gamma+1)\gamma(M-s)^2}{(\gamma-1)\gamma(M-s)^2 + 2\gamma}\Omega - \sqrt{\gamma} M \tag{20}$$

$$\rho_R E_R - \rho_L E_L = \frac{(\gamma+1)\gamma(M-s)^2}{(\gamma-1)\gamma(M-s)^2 + 2\gamma}\Psi - \frac{1}{2}\frac{2 + (\gamma-1)\gamma M^2}{(\gamma-1)}. \tag{21}$$

Here

$$\Omega(M,s) = \sqrt{\gamma} s + \frac{(\gamma-1)\gamma(M-s)^2 + 2\gamma}{(\gamma+1)\sqrt{\gamma}(M-s)}$$

$$\Psi(M,s) = \frac{1}{\gamma-1}\left(\frac{2\gamma(M-s)^2}{\gamma+1} - \frac{\gamma-1}{\gamma+1}\right) + \frac{1}{2}\left(\sqrt{\gamma} s + \frac{(\gamma-1)\gamma(M-s)^2 + 2\gamma}{(\gamma+1)\sqrt{\gamma}(M-s)}\right)^2.$$

For slowly moving shock waves, the jumps in conservative variables given by (19)–(21) have the following asymptotic behavior

$$\rho_R - \rho_L = 2\frac{M^2-1}{\gamma M^2 - M^2 + 2} - 4M\frac{\gamma+1}{(\gamma M^2 - M^2 + 2)^2} s + O(s^2) \tag{22}$$

$$\rho_R u_R - \rho_L u_L = 2\sqrt{\gamma}\frac{M^2-1}{\gamma M^2 - M^2 + 2}s + O(s^2) \tag{23}$$

$$\rho_R E_R - \rho_L E_L = -\frac{A}{\gamma M^2 - M^2 + 2} + \frac{2MB}{(\gamma M^2 - M^2 + 2)^2}s + O(s^2). \tag{24}$$

Here

$$A = \frac{(M-1)(M+1)[(2\gamma^2 - 4\gamma - 2) + (-4\gamma^2 + \gamma^3 - \gamma)M^2]}{(\gamma-1)(\gamma+1)}$$

$$B = \frac{(-4\gamma + 6\gamma^2 - 2) + (4\gamma^3 - 16\gamma^2 - 4\gamma)M^2 + (-5\gamma^3 + \gamma + \gamma^4 + 3\gamma^2)M^4}{(\gamma-1)(\gamma+1)}.$$

Furthermore, the following inequalities hold

$$\begin{cases} \rho_R - \rho_L > 0 \\ \rho_R u_R - \rho_L u_L \to +0, \quad \infty > M > 1, \quad s \to +0 \\ \rho_R E_R - \rho_L E_L > 0 \end{cases} \tag{25}$$

$$\begin{cases} \rho_R - \rho_L < 0 \\ \rho_R u_R - \rho_L u_L \to -0, \quad -\sqrt{\frac{\gamma-1}{2\gamma}} > M > -1, \quad s \to +0. \\ \rho_R E_R - \rho_L E_L < 0 \end{cases} \tag{26}$$

It can be shown that for a right-going shock, the entropy condition in terms of the relative shock speed is given by

$$0 < s < \max(M-1, 0) \quad \text{or } M + \sqrt{\frac{\gamma-1}{2\gamma}} < s < M+1 \tag{27}$$

and a physical shock can move to the right only if $M > -1$.

By (27), it is clear that the only two possible cases to have a slowly and right moving entropy shock are: (a) $M > 1$, (b) $-1 < M < -\sqrt{\frac{\gamma-1}{2\gamma}}$.

For $M > 1$ and $s \to +0$, the flow is supersonic (with small density) in the left and subsonic (with large density) in the right. Hence the condition $\rho_R - \rho_L > 0$ (see Eq. (25)) holds.

For $-\sqrt{\frac{\gamma-1}{2\gamma}} > M > -1$ and $s \to +0$, the flow is supersonic (with small density) in the right and subsonic (with large density) in the left. Hence the condition $\rho_R - \rho_L < 0$ (see Eq. (26)) holds.

3.2. *Sufficient Condition to Avoid Nonphysical Two-Shocked Solution*

For the Euler equations in gas dynamics, the exact form of the Roe matrix at $j + \frac{1}{2}$ is given by [28]

$$\bar{C}_{j+1/2} = \begin{pmatrix} 0 & 1 & 0 \\ \frac{\gamma-3}{2}\bar{u}^2 & (3-\gamma)\bar{u} & \gamma - 1 \\ (\gamma-1)\bar{u}^3 - \gamma\bar{u}\bar{\Theta} + \overline{ua}^2 & \gamma\bar{\Theta} - \bar{a}^2 - \frac{3(\gamma-1)}{2}\bar{u}^2 & \gamma\bar{u} \end{pmatrix},$$

with

$$\bar{u} = \frac{u_j^n + Du_{j+1}^n}{1+D}, \quad \bar{\Theta} = \frac{\Theta_j^n + D\Theta_{j+1}^n}{1+D}, \quad \bar{a}^2 = (\gamma-1)\left(\bar{\Theta} - \frac{1}{2}\bar{u}^2\right). \tag{28}$$

Here $D = \sqrt{\frac{\rho_{j+1}}{\rho_j}}$.

Following Proposition 1, the numerical viscosity $Q_{j+1/2}^n$ is not unique for the case of a system. We shall consider schemes which are as or more dissipative than the Roe scheme. It is thus desirable to use a $Q_{j+1/2}^n$ which has the same eigenvectors as the Roe scheme. This is possible (as will be proved in the next proposition) since there is an infinite number of numerical viscosity $Q_{j+1/2}^n$ satisfying (9). For convenience, let us define $|\bar{C}_{j+1/2}|$ by

$$\left|\bar{C}_{j+1/2}\right| = \bar{L}_{j+1/2}\left|\bar{\Lambda}_{j+1/2}\right|\bar{L}_{j+1/2}^{-1},$$

with $|\bar{\Lambda}| = \mathrm{diag}(|\bar{u}|, |\bar{u}+\bar{a}|, |\bar{u}-\bar{a}|)$ and the diagonalization matrices are still given by (15) and (16) with their arguments u, Θ and a replaced by the Roe averages $\bar{u}$, $\bar{\Theta}$, and $\bar{a}$ defined in (28).

PROPOSITION 2. *There is a diagonal matrix $\Lambda_{j+1/2}^{(p)}$ such that the numerical viscosity $Q_{j+1/2}^n$ satisfies both* (9) *and the following relation*

$$Q_{j+1/2}^n = \left|\bar{C}_{j+1/2}\right| + \bar{L}_{j+1/2}\Lambda_{j+1/2}^{(p)}\bar{L}_{j+1/2}^{-1}. \tag{29}$$

Proof. Inserting (29) into (9) yields

$$G_{j+1/2}^n = \frac{1}{2}\left(H_j^n + H_{j+1}^n\right) + \frac{1}{2}\left(\left|\bar{C}_{j+1/2}\right| + \bar{L}_{j+1/2}\Lambda_{j+1/2}^{(p)}\bar{L}_{j+1/2}^{-1}\right)\left(V_j^n - V_{j+1}^n\right),$$

which can also be written as

$$\Lambda_{j+1/2}^{(p)}\bar{L}_{j+1/2}^{-1}\left(V_j^n - V_{j+1}^n\right) = \bar{L}_{j+1/2}^{-1}\left[2G_{j+1/2}^n - \left(H_j^n + H_{j+1}^n\right) - \left|\bar{C}_{j+1/2}\right|\left(V_j^n - V_{j+1}^n\right)\right]$$

or

$$\begin{pmatrix} q^{(1)}\varphi^{(1)} \\ q^{(2)}\varphi^{(2)} \\ q^{(3)}\varphi^{(3)} \end{pmatrix} = \bar{L}_{j+1/2}^{-1}\left[2G_{j+1/2}^n - \left(H_j^n + H_{j+1}^n\right) - \left|\bar{C}_{j+1/2}\right|\left(V_j^n - V_{j+1}^n\right)\right], \tag{30}$$

where $q^{(k)}$ is the kth component of the column vector $\bar{L}_{j+1/2}^{-1}(V_j^n - V_{j+1}^n)$ and $\varphi^{(k)}$ is the kth diagonal element of $\Lambda_{j+1/2}^{(p)}$.

Since $G_{j+1/2}^n$, $\frac{1}{2}(H_j^n + H_{j+1}^n)$, $|\bar{C}_{j+1/2}|$, $\bar{L}_{j+1/2}$, $\bar{L}_{j+1/2}^{-1}$ and $(V_j^n - V_{j+1}^n)$ are all known functions for a given scheme, Eq. (30) defines three relations for the three unknowns in the diagonal matrix $\Lambda_{j+1/2}^{(p)}$. Hence there is always a matrix $\Lambda_{j+1/2}^{(p)}$ satisfying (9) and (29). ■

Remark 3.1. If one just looks at (29), then one would get an impression that (29) would not be true since $Q_{j+1/2}^n$ has $m \times m$ elements while $\Lambda_{j+1/2}^{(p)}$ only has m elements. This is because combining (9) and (29) yields m relations for the m unknowns in $\Lambda_{j+1/2}^{(p)}$. Since there is an infinite number of $Q_{j+1/2}^n$ satisfying (9), it is always possible to have a $Q_{j+1/2}^n$ satisfying both (9) and (29), and particularly having the same eigenvectors as the Roe matrix.

Remark 3.2. If we further assume that the two points j and $j+1$ cross a very slowly right-moving shock, then $(V_j^n - V_{j+1}^n)$ defines the jump across the shock. Hence we can use (15) and (22)–(24) to compute the expression for each $q^{(k)}$. Consider for instance $q^{(3)}$. A direct calculation similar to the proof for Proposition 3 shows that

$$q^{(3)} = \bar{l}_{1/2}^{(31)} o^{(1)} + \bar{l}_{1/2}^{(33)} o^{(3)} + O(s) > 0$$

for small s. Here $\bar{l}_{1/2}^{(mn)}$ is the element of $\bar{L}_{1/2}^{-1}$ in row m and in column n and $o^{(k)}$ is the kth element of $(V_j^n - V_{j+1}^n)$. Similarly, we have $q^{(1)} \neq 0$ and $q^{(2)} \neq 0$. Hence $q^{(k)} \neq 0$ for $k = 1, 2, 3$, and the matrix $\Lambda_{j+1/2}^{(p)}$ is unique.

Remark 3.3. The matrix $\bar{L}_{j+1/2} \Lambda_{j+1/2}^{(p)} \bar{L}_{j+1/2}^{-1}$ represents a difference of the numerical viscosity between the considered numerical scheme and the standard first-order accurate Roe scheme with $Q_{j+1/2}^n = |\bar{C}_{j+1/2}|$ or $\Lambda_{j+1/2}^{(p)} = 0$.

DEFINITION. A numerical scheme is said to be no less dissipative than the standard Roe scheme if none of the diagonal elements of $\Lambda_{j+1/2}^{(p)}$ is negative.

Now we are able to prove the main result of this paper. In order to avoid complication, we make the restriction $u_L > 0$ in the statement of this result. In the next section we will simply explain that this condition can be removed.

PROPOSITION 3. *For the Euler equations in gas dynamics, if just at the moment that the right-going shock coincides with the left interface, the numerical dissipation coefficient $Q_{1/2}$ of the interior difference equation is no smaller than the standard Roe scheme, then a slowly right-going shock wave with $u_L > 0$ will not stick to the interface in the form of a two-shocked steady state even though the interpolation is defined by nonconservative normal interpolations.*

Proof. With the definition (29), the basic condition of two-shocked solution (14) can be rewritten as

$$\frac{1}{2}\left(|\bar{C}_{1/2}| + \bar{L}_{1/2} \Lambda_{1/2}^{(p)} \bar{L}_{1/2}^{-1} - \bar{C}_{1/2}\right)(W_L - V_1) = s(W_R - W_L)$$

or equivalently

$$\left(|\bar{\Lambda}_{1/2}| + \Lambda_{1/2}^{(p)} - \bar{\Lambda}_{1/2}\right) \bar{L}_{1/2}^{-1} (W_L - V_1) = 2s \bar{L}_{1/2}^{-1} (W_R - W_L). \tag{31}$$

Now we want to prove that (31) does not hold. Let $\bar{l}_{1/2}^{(mn)}$ be the element of $\bar{L}_{1/2}^{-1}$ in row m and in column n. Let $w^{(m)}$ be the mth component of $W_R - W_L$ and $v^{(m)}$ be the mth component of $W_L - V_1$. It suffices to prove that (31) does not hold for one component. Consider the third component for which (31) takes the following form

$$\bar{\lambda}^{(3)} \bar{l}_{1/2}^{(3n)} v^{(n)} = 2s \bar{l}_{1/2}^{(3n)} w^{(n)}, \tag{32}$$

where $\bar{\lambda}^{(3)}$ is the third element of $(|\bar{\Lambda}_{1/2}| + \Lambda_{1/2}^{(p)} - \bar{\Lambda}_{1/2})$. By assumption that $Q_{1/2}$ is no smaller than the standard Roe scheme at the moment of shock/interface interaction, we have

$$\bar{\lambda}^{(3)} \geq 0. \tag{33}$$

By (15), we have

$$\bar{l}^{(31)}_{1/2} = -\bar{u}_{1/2} - \frac{1}{2\bar{a}_{1/2}}(\gamma - 1)\,\bar{u}^2_{1/2}$$

$$\bar{l}^{(32)}_{1/2} = 1 + \frac{1}{\bar{a}_{1/2}}(\gamma - 1)\,\bar{u}_{1/2}$$

$$\bar{l}^{(33)}_{1/2} = -\frac{1}{\bar{a}_{1/2}}(\gamma - 1).$$

Thus $\bar{l}^{(32)}_{1/2} > 0$ and

$$\bar{l}^{(31)}_{1/2} < 0, \quad \bar{l}^{(33)}_{1/2} < 0. \tag{34}$$

If the shock gets stuck at the left interface, then V_1 lies at the middle of W_L and W_R or goes over W_R (in case of numerical oscillation), so that

$$sgn\big(v^{(n)}\big) = -sgn\big(w^{(n)}\big) \quad \forall n \in \{1, 2, 3\}. \tag{35}$$

According to the asymptotic behavior (22)–(24), $w^{(1)}$ and $w^{(3)}$ have the same sign and are bounded from zero, while $w^{(2)}$ vanishes at the speed $O[s]$ for $s \to 0$. Thus for a very slow shock with $s \to 0$ but $s \neq 0$, (32) reduces to

$$\bar{\lambda}^{(3)}\Big(\bar{l}^{(31)}_{1/2} v^{(1)} + \bar{l}^{(33)}_{1/2} v^{(3)} + O(s)\Big) = 2s\Big(\bar{l}^{(31)}_{1/2} w^{(1)} + \bar{l}^{(33)}_{1/2} w^{(3)} + O(s)\Big). \tag{36}$$

By the inequalities (25), (26), (33), (34), and (35), we have

$$\begin{cases} s\Big(\bar{l}^{(31)}_{1/2} w^{(1)} + \bar{l}^{(33)}_{1/2} w^{(3)} + O(s)\Big) > 0 \\ \bar{\lambda}^{(3)}\Big(\bar{l}^{(31)}_{1/2} v^{(1)} + \bar{l}^{(33)}_{1/2} v^{(3)} + O(s)\Big) \le 0 \end{cases} \quad \text{for } M > 1$$

$$\begin{cases} s\Big(\bar{l}^{(31)}_{1/2} w^{(1)} + \bar{l}^{(33)}_{1/2} w^{(3)} + O(s)\Big) > 0 \\ \bar{\lambda}^{(3)}\Big(\bar{l}^{(31)}_{1/2} v^{(1)} + \bar{l}^{(33)}_{1/2} v^{(3)} + O(s)\Big) \le 0 \end{cases} \quad \text{for } 0 < M < 1$$

so that the condition (36) does not hold for a right-going shock with small $s > 0$.

Thus the basic condition of two-shocked solution does not hold. This completes the proof. ■

Remark 3.4. In Proposition 3 we have required the restriction for $Q_{1/2}$ just at the moment that the right-going shock coincides with the left interface. This means that there is no restriction for the numerical viscosity at the points other than the interface point or at the time when the shock is not at the interface point.

Remark 3.5. In the limit case $s = 0$, $\bar{\lambda}^{(3)}$ could vanish inside the shock so that condition (36) holds. This is not a contradiction since a steady shock should remain where it is.

3.3. *Discussion*

The condition stated in Proposition 3 is a sufficient condition and not a necessary one. Thus in practice a numerical scheme having slightly less numerical dissipation than the standard Roe scheme may also work.

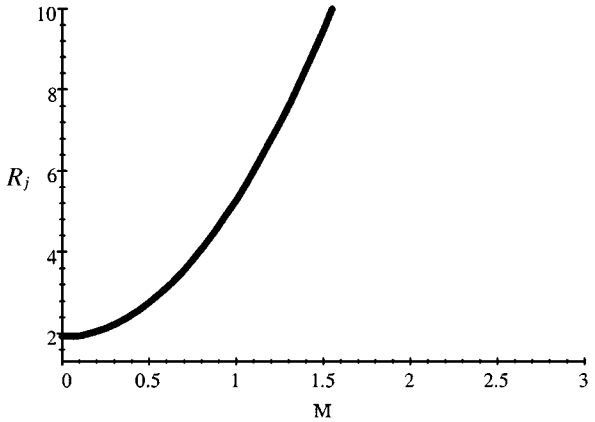

FIG. 6. Ratio (R_j) between the jump in total engery and the jump in density in function of the Mach number.

The extension of the scalar result to the system of Euler equations in gas dynamics lies heavily on the structure of slowly moving shock waves, for which the momentum jump vanishes with vanishing shock speed and while the jumps in density and in total energy keep finite values for vanishing shock speed. This allows us to prove that the basic condition of the two-shocked solution does not hold. But we are actually unable to extend the results to a general hyperbolic system of conservation laws.

Since the condition stated in Proposition 3 is required only locally at the point of shock/interface interaction, one may construct a local penetrator for schemes not satisfying such a condition. For example, the Lax–Wendroff scheme does not satisfy the dissipation requirement $\Lambda^{(p)}_{j+1/2} \geq 0$. To ensure shock interface penetration, one can simply perturb the

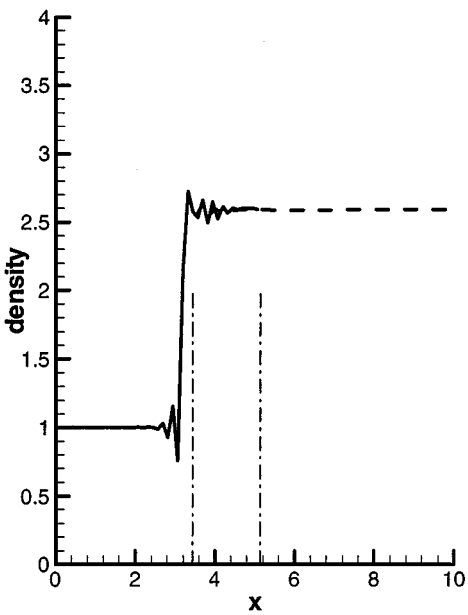

FIG. 7. Computed shock at instant $t = t_{left}$. Lax–Wendroff scheme for $M = 2$, $s = 0.05$.

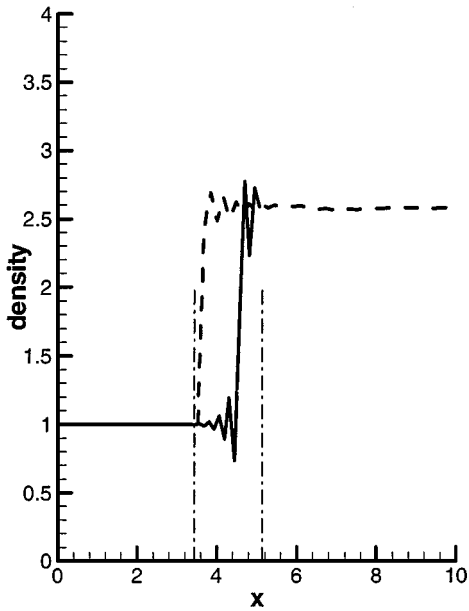

FIG. 8. Computed shock at instant $t = t_{middle}$. Lax–Wendroff scheme for $M = 2, s = 0.05$.

interface value $Q^n_{1/2}$ by setting $Q^n_{1/2} = |\bar{C}_{1/2}|$ just at the moment of shock passing at the interface. Such a penetrator is even easier than the penetrator stated in [36].

The restriction $u_L > 0$ in Proposition 3 can be removed. In fact, for $u_L < 0,$ the inequalities (34) are replaced by

$$\bar{l}^{(31)}_{1/2} > 0, \qquad \bar{l}^{(33)}_{1/2} < 0.$$

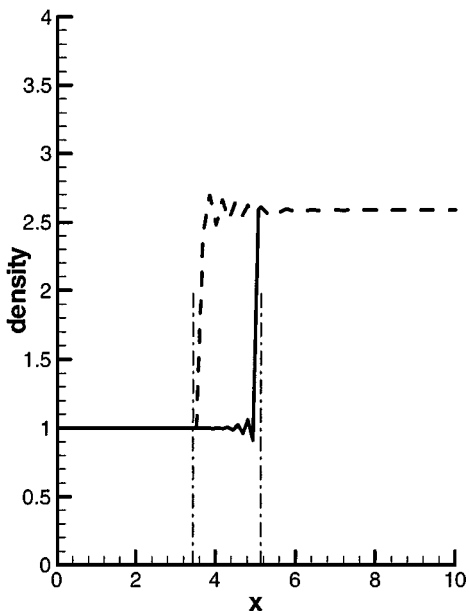

FIG. 9. Computed shock at instant $t = t_{right}$. Lax–Wendroff scheme for $M = 2, s = 0.05$.

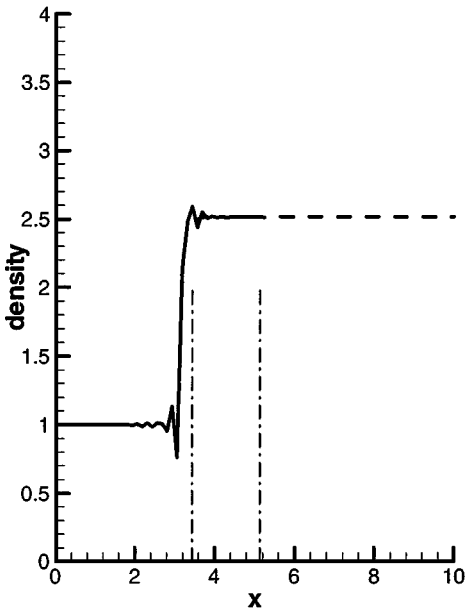

FIG. 10. Computed shock at instant $t = t_{left}$. Lax–Wendroff scheme for $M = 2, s = 0.1$.

From (22) and (24) it can be shown that for vanishing shock speed, we have

$$\frac{w^{(3)}}{w^{(1)}} = \frac{\rho_R E_R - \rho_L E_L}{\rho_R - \rho_L} > 1.916\,7$$

and the dependence of $\frac{w^{(3)}}{w^{(1)}}$ at $s \to 0$ for various negative Mach numbers is displayed in Fig. 6. Thus the third component $w^{(3)}$ dominates the first component $w^{(1)}$, and the sign of

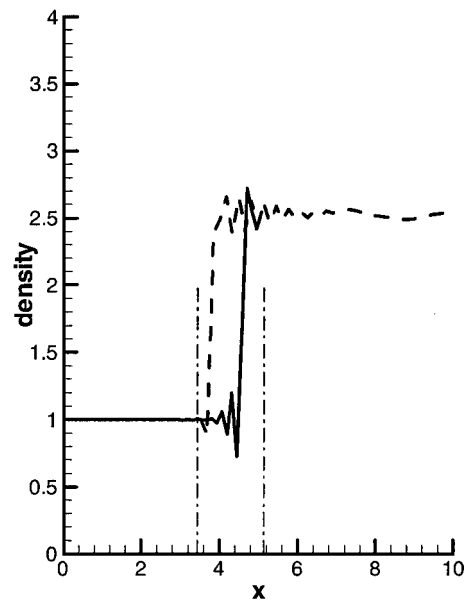

FIG. 11. Computed shock at instant $t = t_{middle}$. Lax–Wendroff scheme for $M = 2, s = 0.1$.

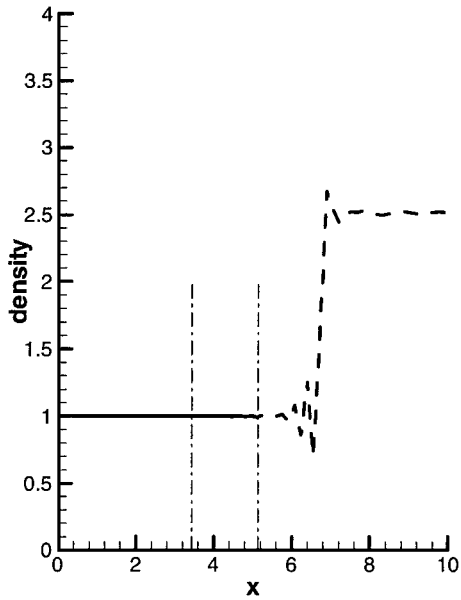

FIG. 12. Computed shock at instant $t = t_{right}$. Lax–Wendroff scheme for $M = 2, s = 0.1$.

the left- and right-hand sides of (36) is dominated by the factor with $w^{(3)}$ in such a way that one can still prove that (36) does not hold. Still using this property, one can show that the first two components of (31) do not hold.

Modern high resolution schemes equipped with limiters, nonlinear filters, or large artificial dissipation should satisfy the sufficient condition stated in Proposition 3. Thus the overlapping grid treatment using high resolution schemes and nonconservative normal interpolation works in practice.

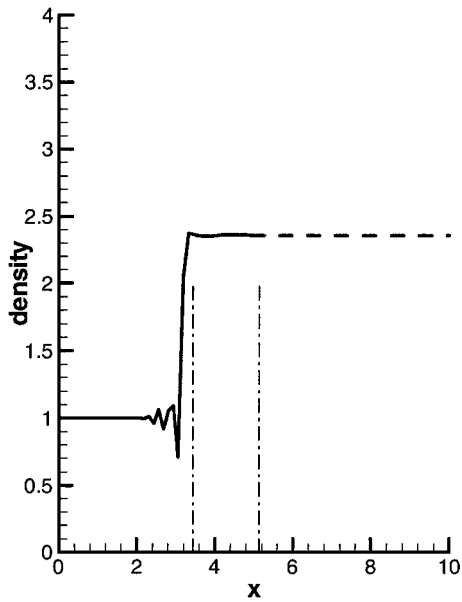

FIG. 13. Computed shock at instant $t = t_{left}$. Lax–Wendroff scheme for $M = 2, s = 0.2$.

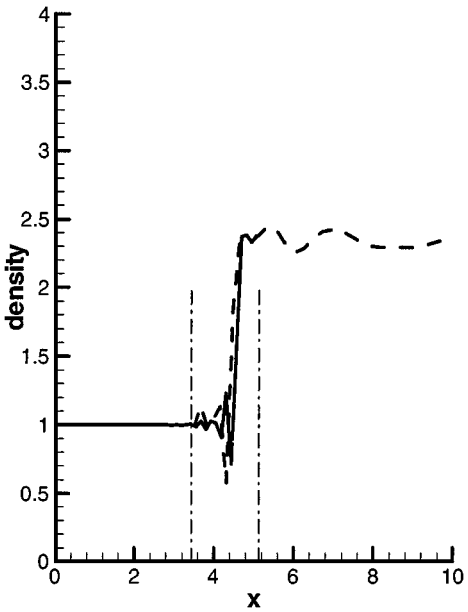

FIG. 14. Computed shock at instant $t = t_{middle}$. Lax–Wendroff scheme for $M = 2$, $s = 0.2$.

4. NUMERICAL RESULTS

In [36], which is essentially a scalar study, we have already displayed a few numerical results for the Euler equations in gas dynamics. Here we display further numerical results for the case of system, by considering more shock speeds and stronger shock waves.

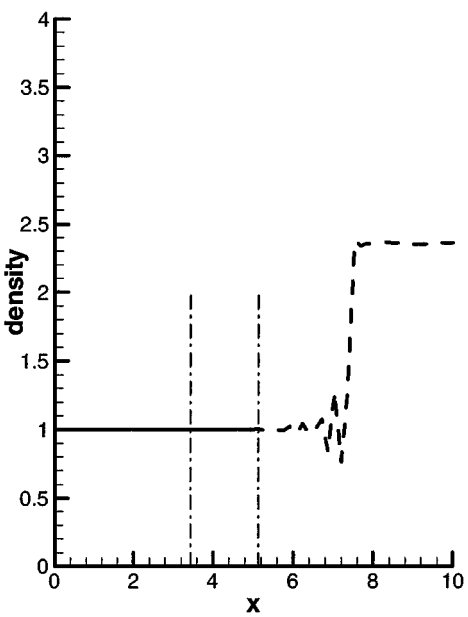

FIG. 15. Computed shock at instant $t = t_{right}$. Lax–Wendroff scheme for $M = 2$, $s = 0.2$.

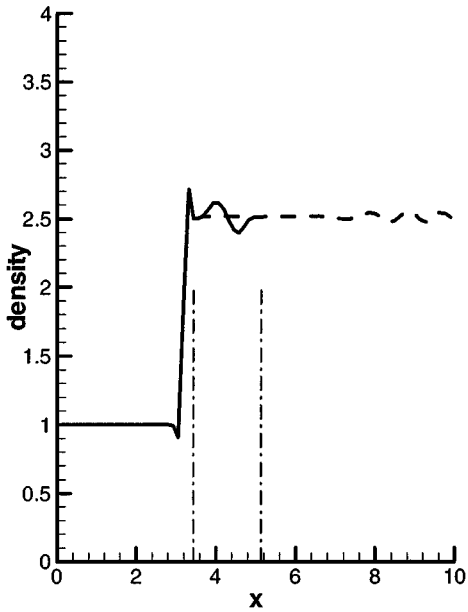

FIG. 16. Computed shock at instant $t = t_{left}$. MUSCL scheme wihout limiter for $M = 2, s = 0.1$.

We consider four typical schemes: (1) first-order Roe scheme (Roe), (2) first-order van Leer scheme having a numerical viscosity slightly greater than that of the Roe scheme, (3) second-order Lax–Wendroff scheme having a numerical viscosity smaller than the Roe scheme, and (4) second-order MUSCL scheme (MUSCL) integrated in time by a fourth-order Runge–Kutta method. The first three schemes are well documented in [11] and need not be repeated here. For the case of the MUSCL scheme, we use the following numerical

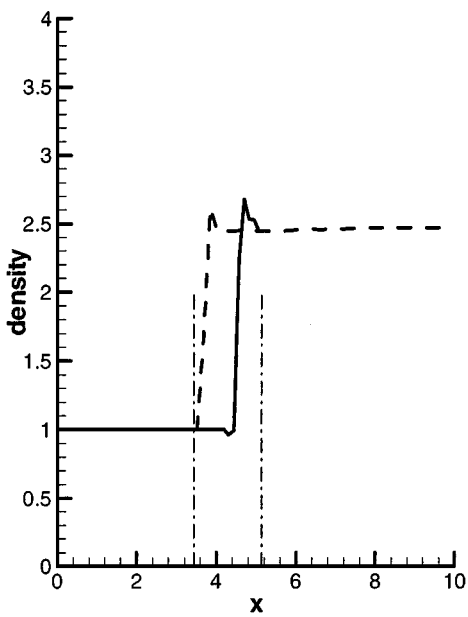

FIG. 17. Computed shock at instant $t = t_{middle}$. MUSCL scheme wihout limiter for $M = 2, s = 0.1$.

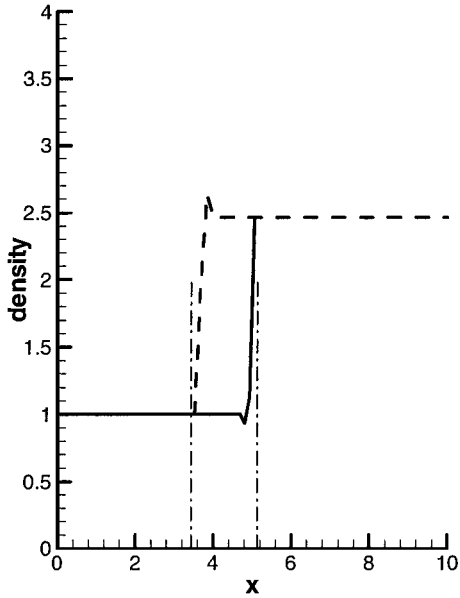

FIG. 18. Computed shock at instant $t = t_{right}$. MUSCL scheme wihout limiter for $M = 2, s = 0.1$.

flux for the left subdomain

$$F^n_{j+1/2} = H^+\big(w^n_{lft}\big) + H^-\big(w^n_{rgt}\big),$$

where $w^n_{lft} = w^n_j + \frac{1}{2}\varphi(w^n_j - w^n_{j-1})$ and $w^n_{rgt} = w^n_{j+1} - \frac{1}{2}\varphi(w^n_{j+1} - w^n_j)$. Here H^+ and H^- are characteristic decompositions of the flux H according to the positive and negative

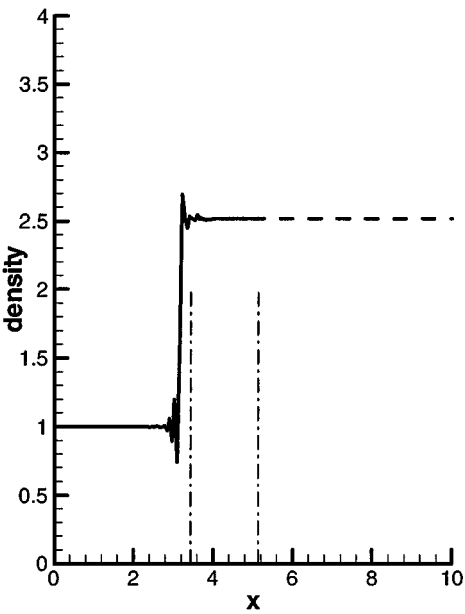

FIG. 19. Computed shock at instant $t = t_{left}$. The mesh is refined one times. Lax–Wendroff scheme for $M = 2, s = 0.1$.

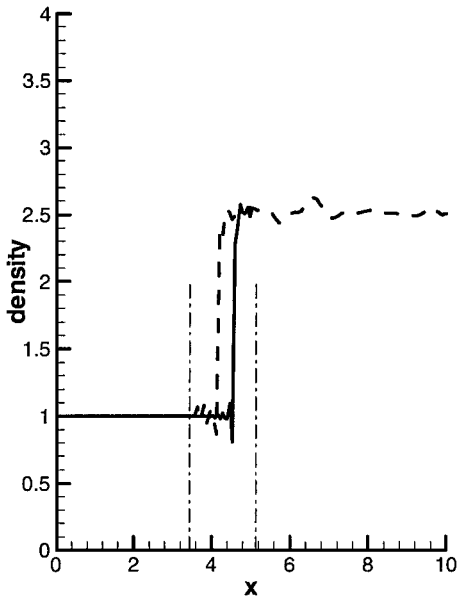

FIG. 20. Computed shock at instant $t = t_{middle}$. The mesh is refined one times. Lax–Wendroff scheme for $M = 2, s = 0.1$.

eigenvalues of the Jacobian matrix, and φ is a slope limiter. In the case without limiter, $\varphi = 1$. In the case with limiter, we choose the well-known minmod limiter. The flux $G^n_{j+1/2}$ for the right subdomain can be similarly defined.

The computational domain is split as: $D_u = \{x : 0 < x < 5\}$, $D_v = \{x : 3.6 < x < 10\}$. There are 40 uniform meshes in each subdomain unless otherwise stated. We output the

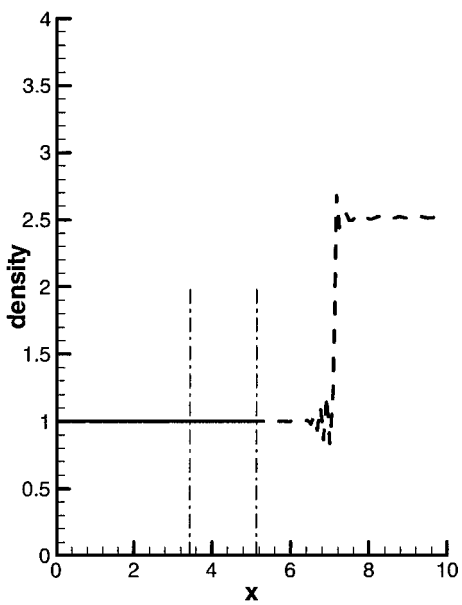

FIG. 21. Computed shock at instant $t = t_{right}$. The mesh is refined one time. Lax–Wendroff scheme for $M = 2, s = 0.1$.

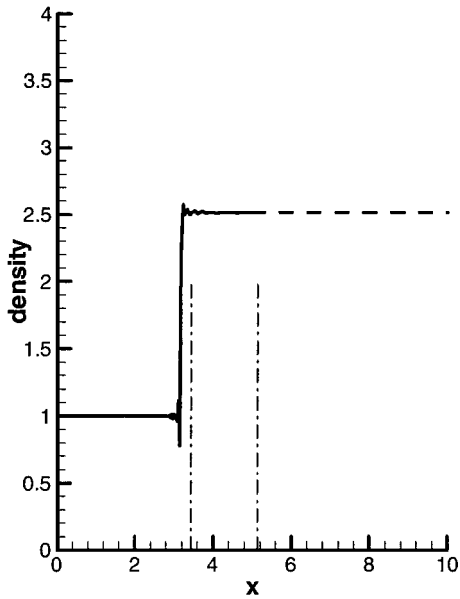

FIG. 22. Computed shock at instant $t = t_{left}$. The mesh is refined two times. Lax–Wendroff scheme for $M = 2, s = 0.1$.

solutions at three instants: $t = t_{left}, t_{middle}, t_{right}$, corresponding to a shock (exact) position $x = 3.3 < -a$, $-a < x = 4.5 < b$, and $x = 7 > b$. In all computations we use $CFL = 0.80$. Using other kinds of decomposition leads to similar results. Only the nonconservative normal interpolation will be used at the interface. The Berger's flux interpolation has been rigorously shown to yield conservative results and will not be reconsidered here.

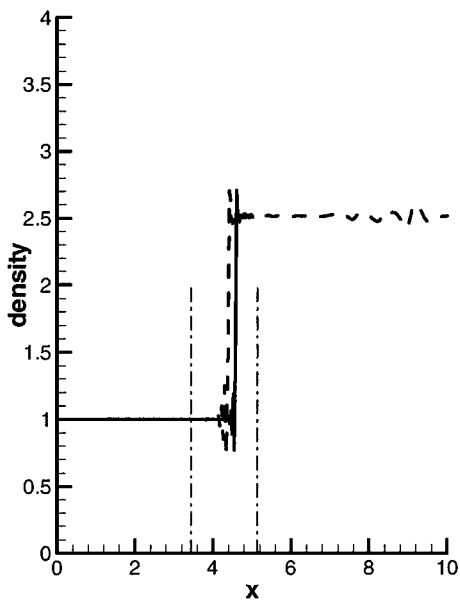

FIG. 23. Computed shock at instant $t = t_{middle}$. The mesh is refined two times. Lax–Wendroff scheme for $M = 2, s = 0.1$.

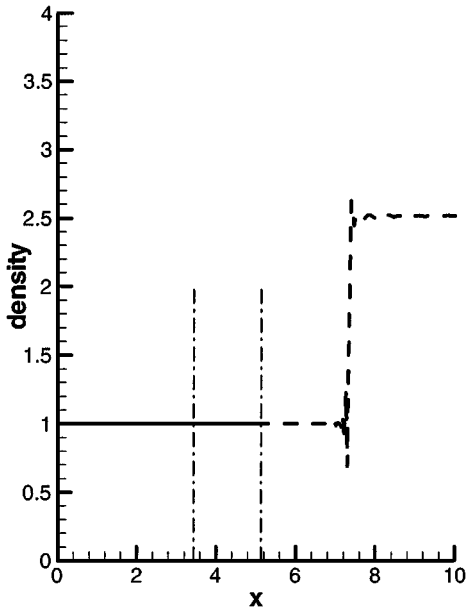

FIG. 24. Computed shock at instant $t = t_{right}$. The mesh is refined two times. Lax–Wendroff scheme for $M = 2, s = 0.1$.

Let $\rho_L = 1$, $p_L = 1$, and $u_L = \sqrt{\gamma}M$, where M is the Mach number in the left of the shock wave. Then the right-hand states of the shock are related to the shock speed s by

$$u_R = \sqrt{\gamma}s + \sqrt{\gamma}\frac{(\gamma - 1)(M - s)^2 + 2}{(\gamma + 1)(M - s)} \tag{37}$$

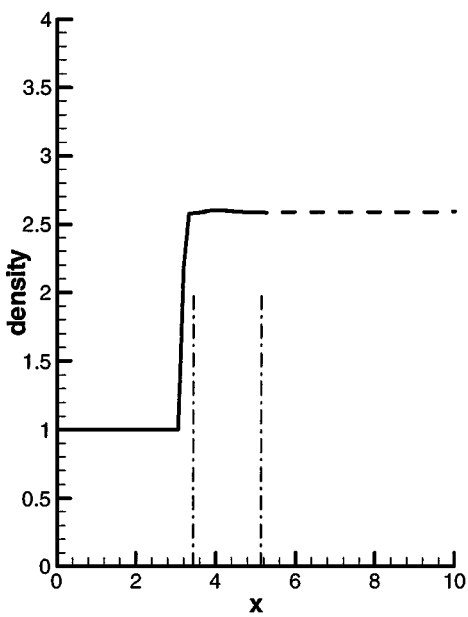

FIG. 25. Computed shock at instant $t = t_{left}$. Roe scheme for $M = 2, s = 0.05$.

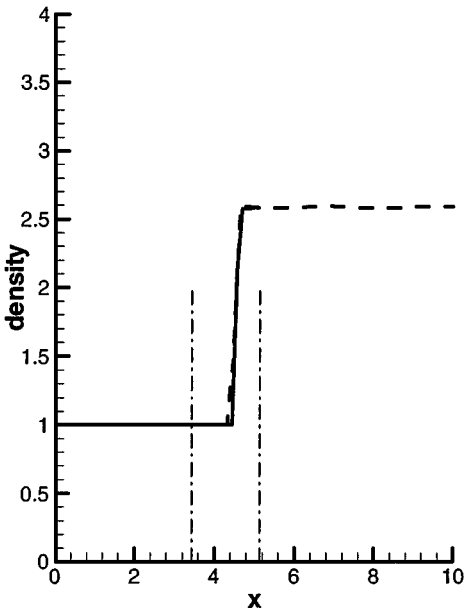

FIG. 26. Computed shock at instant $t = t_{middle}$. Roe scheme for $M = 2,\ s = 0.05$.

$$\rho_R = \frac{(\gamma+1)\gamma(M-s)^2}{(\gamma-1)\gamma(M-s)^2+2\gamma} \tag{38}$$

$$p_R = \frac{2\gamma(M-s)^2}{\gamma+1} - \frac{\gamma-1}{\gamma+1}. \tag{39}$$

The initial shock lies at $x = 3.16$.

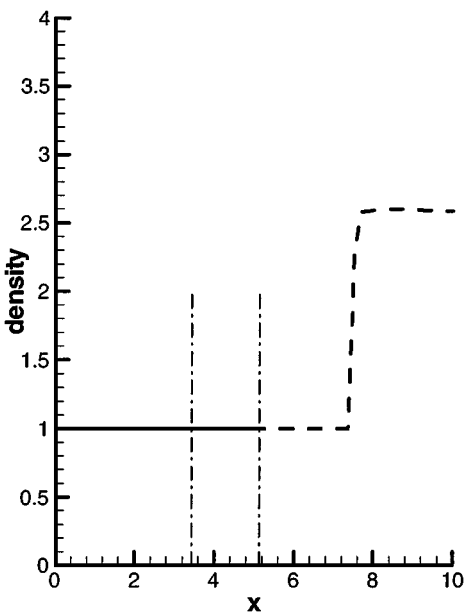

FIG. 27. Computed shock at instant $t = t_{right}$. Roe scheme for $M = 2,\ s = 0.05$.

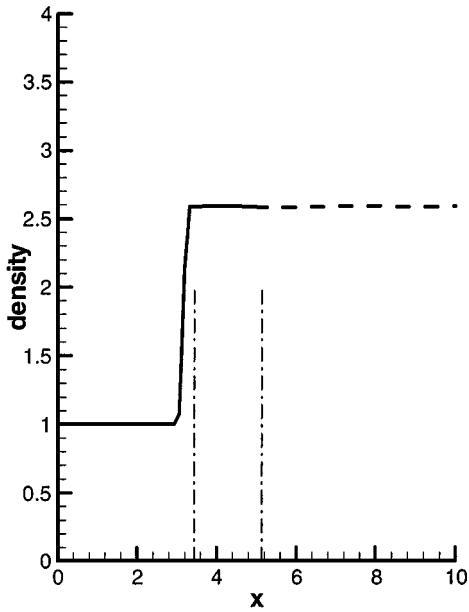

FIG. 28. Computed shock at instant $t = t_{left}$. van Leer scheme for $M = 2,\ s = 0.05$.

4.1. *Transmission for Weakly Dissipative Schemes*

We begin with the Lax–Wendroff scheme which is less dissipative than the Roe scheme. The Mach number is fixed to be $M = 2$.

For $s = 0.05$, the computed density is displayed in Figs. 7–9. For these figures and for the subsequent figures, the solution is displayed as a solid line in the left subdomain and a dashed line in the right subdomain. We also displayed two vertical, dot-dashed lines to show

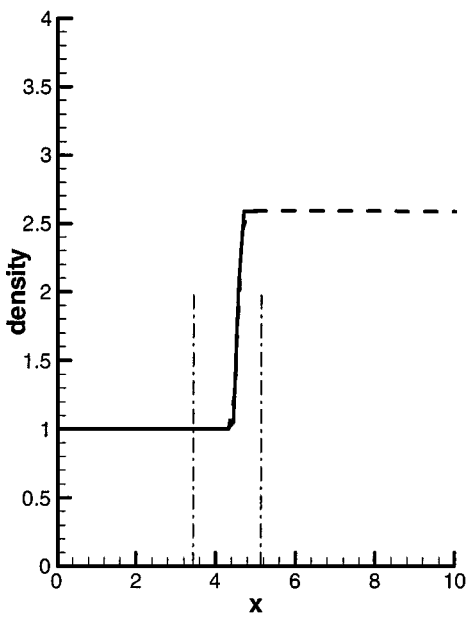

FIG. 29. Computed shock at instant $t = t_{middle}$. van Leer scheme for $M = 2,\ s = 0.05$.

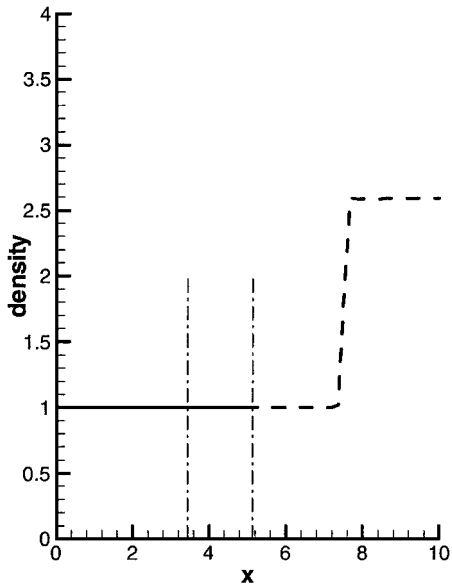

FIG. 30. Computed shock at instant $t = t_{right}$. van Leer scheme for $M = 2$, $s = 0.05$.

the two boundaries of the overlap. At $t = t_{left}$, the numerical shock is in the left of the overlap (Fig. 7). At $t = t_{middle}$, where the exact shock should lie at $x = 4.5$, the numerical shocks inside both subdomains do not lie at the same position: Shock R sticks to the left boundary of the overlap, and Shock L reaches the exact shock position ($x = 4.5$). At $t = t_{right}$, the exact shock lies at $x = 7$, while the numerical solution reaches a nonphysical, two-shocked steady state. Hence for the Lax–Wendroff scheme, a very slowly moving shock fails to transmit the grid interface and attains a nonphysical, two-shocked steady state.

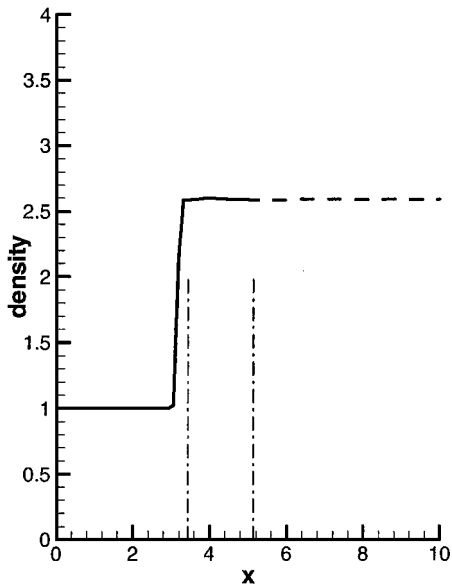

FIG. 31. Computed shock at instant $t = t_{left}$. MUSCL schemes with minmod limiter for $M = 2$, $s = 0.05$.

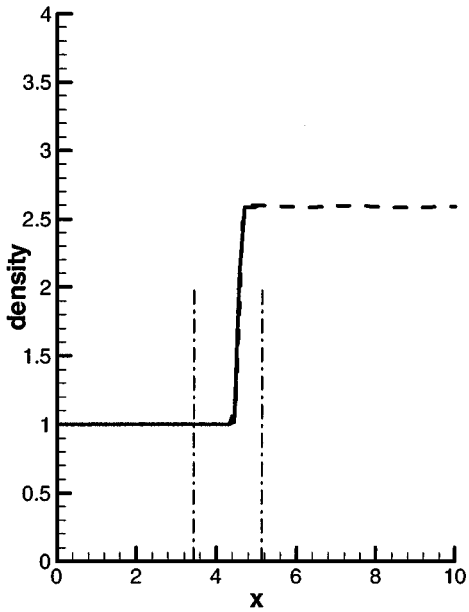

FIG. 32. Computed shock at instant $t = t_{middle}$. MUSCL schemes with minmod limiter for $M = 2$, $s = 0.05$.

For $s = 0.1$, the computed density is displayed in Figs. 10–12. At $t = t_{middle}$, where the exact shock should lie at $x = 4.5$, we still observe that Shock L and Shock R do not lie at the same position. But this time Shock R lags a distance with respect to Shock L and does not stick to the interface. At $t = t_{right}$, the exact shock lies at $x = 7$, while the numerical shock is near 6.5. Hence for sufficiently high shock speed, the shock can transmit the interface, but with a strong delay.

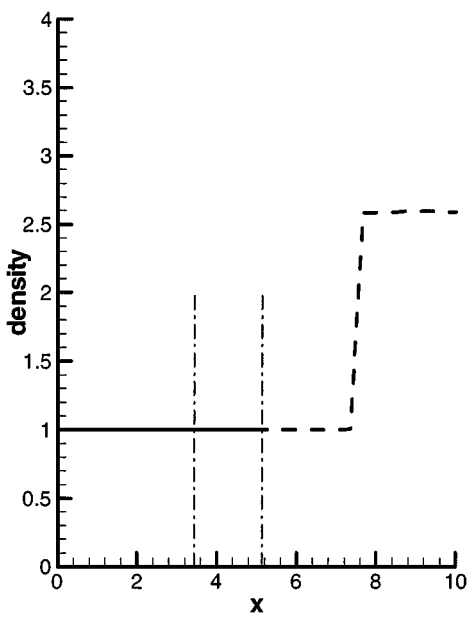

FIG. 33. Computed shock at instant $t = t_{right}$. MUSCL schemes with minmod limiter for $M = 2$, $s = 0.05$.

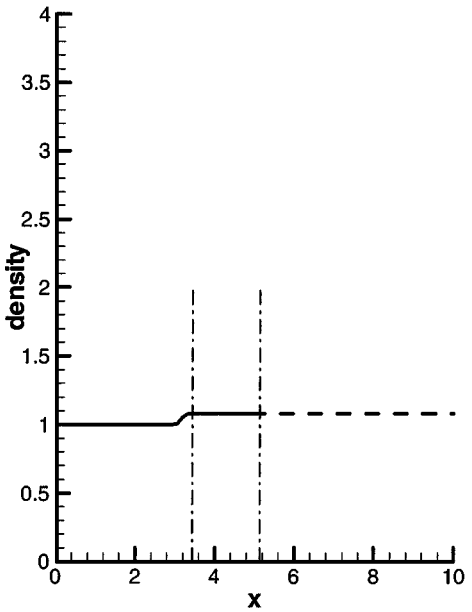

FIG. 34. Computed shock at instant $t = t_{left}$. van Leer scheme for a weak shock with $M = 1.1,\ s = 0.05$.

For $s = 0.2$, the computed density is displayed in Figs. 13–15. At $t = t_{middle}$, where the exact shock should lie at $x = 4.5$, we observe that Shock L and Shock R lie at the same position. At $t = t_{right}$, the numerical shock reaches the position of the exact shock. Hence for large shock speed, the shock can transmit the interface without delay.

Now consider the MUSCL scheme without limiter. The computed density for $s = 0.1$ is displayed in Figs. 16–18. We have shown that for the Lax–Wendroff scheme the shock is

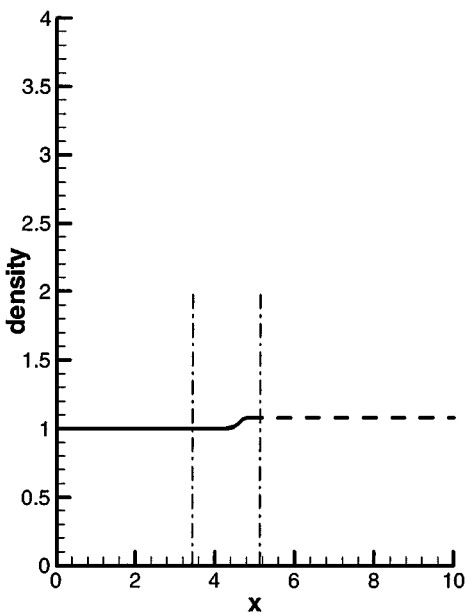

FIG. 35. Computed shock at instant $t = t_{middle}$. van Leer scheme for a week shock with $M = 1.1,\ s = 0.05$.

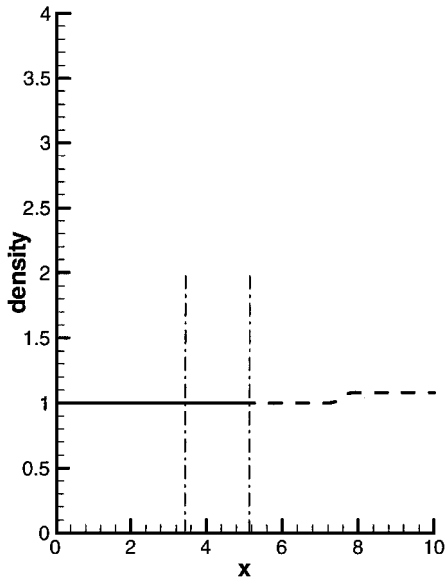

FIG. 36. Computed shock at instant $t = t_{right}$. van Leer scheme for a week shock with $M = 1.1,\ s = 0.05$.

able to transmit the interface, though with a delay. But here for the MUSCL scheme the shock fails to transmit by producing a two-shocked solution. Hence we need higher shock speed for transmission for the MUSCL scheme.

4.2. *Error Reduction by Mesh Refinement for Delayed Transmission*

Now we want to see whether the conservation error in the case of transmission delay can be made as small as we require by reducing the mesh size. We consider the Lax–Wendroff

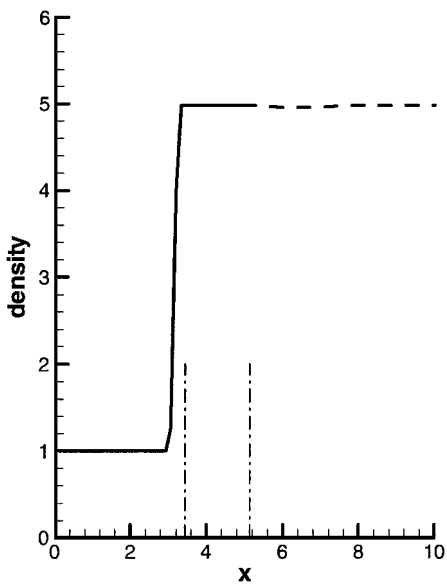

FIG. 37. Computed shock at instant $t = t_{left}$. van Leer scheme for a strong shock with $M = 5,\ s = 0.05$.

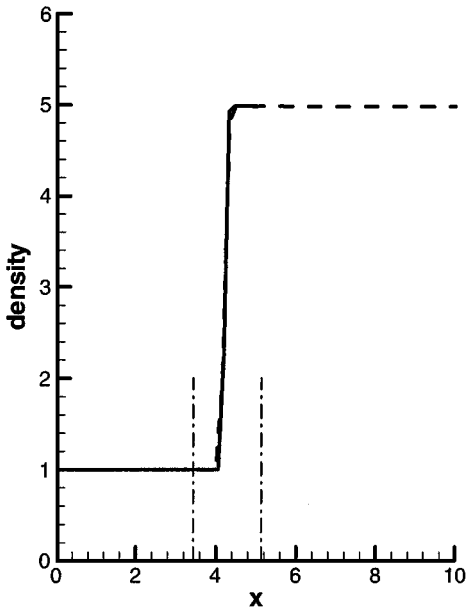

FIG. 38. Computed shock at instant $t = t_{middle}$. van Leer scheme for a strong shock with $M = 5$, $s = 0.05$.

scheme for $M = 2$ and $s = 0.1$. In this case there is delayed transmission, as shown in Figs. 10–12.

Now we refine the grid one time, so that there were 80 mesh points in each subdomain. The computed density is displayed in Figs. 19–21. We still observe a delay, but the delayed distance is reduced two times.

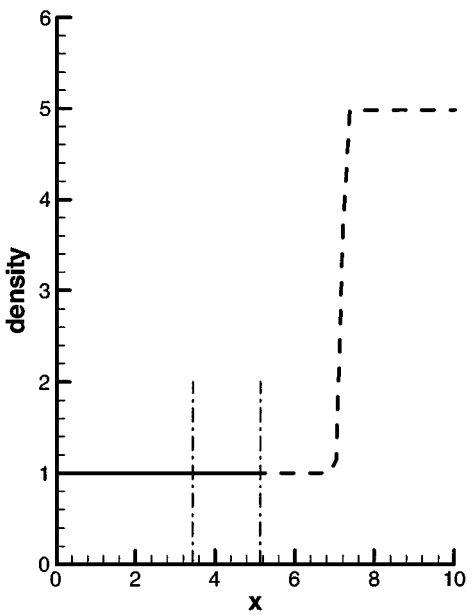

FIG. 39. Computed shock at instant $t = t_{right}$. van Leer scheme for a strong shock with $M = 5$, $s = 0.05$.

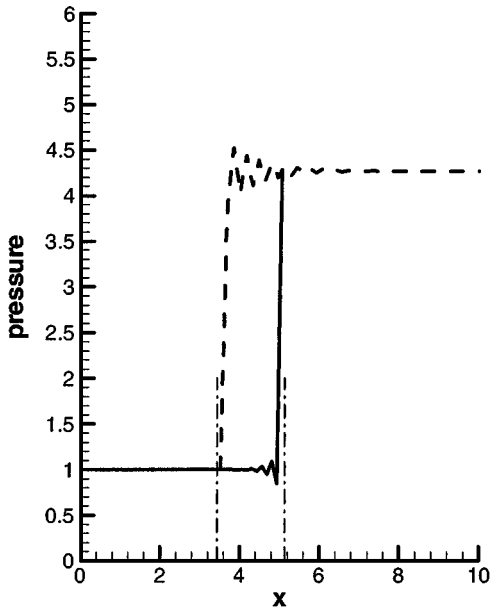

FIG. 40. Computed pressure at instant $t = t_{right}$. Lax–Wendroff scheme for $M = 2, s = 0.05$.

Finally we refine the grid two times, so that there were 160 mesh points in each subdomain. The computed density is displayed in Figs. 22–24. In comparison with Figs. 10–12, the delayed distance is reduced four times.

Hence for delayed transmission, the error of the shock location can be reduced by refining the mesh as much as we require.

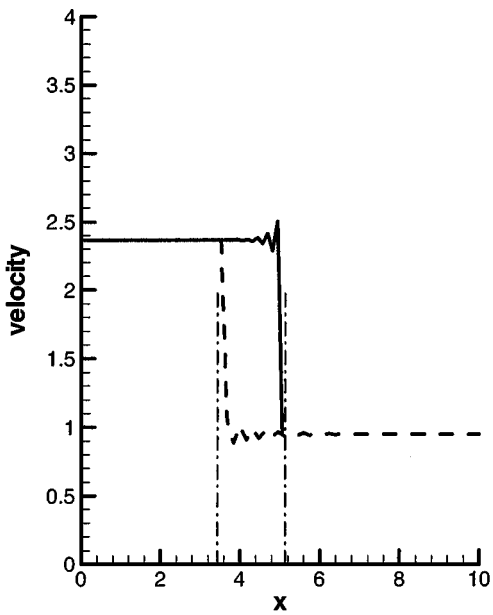

FIG. 41. Computed velocity at instant $t = t_{right}$. Lax–Wendroff scheme for $M = 2, s = 0.05$.

4.3. *Transmission for Strongly Dissipative Schemes*

Now we consider the first-order Roe scheme, the van Leer scheme, and the MUSCL scheme with limiter. In these cases the scheme is at least as dissipative as the Roe scheme inside the shock. We consider $M = 2$ and $s = 0.05$, for which the weakly dissipative schemes fail to work.

The computed density for the Roe scheme is displayed in Figs. 25–27. We observe perfect transmission. For the van Leer scheme which is slightly more dissipative than the Roe scheme, we still observe perfect transmission as displayed in Figs. 28–30. Using the MUSCL scheme with limiter, the scheme reduced to first-order inside the shock, so that we also have perfect transmission as displayed in Figs. 31–33.

Hence for schemes no less dissipative than the Roe scheme (inside the shock), no steady-state two-shocked solution occurs, no observable transmission delay occurs.

4.4. *Transmission with Various Shock Strengths*

The shock strength can be defined as p_R/p_L, which depends on both M and s, as can be seen from (39). The case with various s has already been discussed. Here we vary the Mach number and simply use the van Leer scheme. The shock speed is fixed to be $s = 0.05$.

First consider a weak shock with $M = 1.1$. The computed density is displayed in Figs. 34–36. The shock transmits the interface perfectly, as for the case of a middle strength shock (Figs. 28–30).

Now consider a more strong shock with $M = 5$. The computed density is displayed in Figs. 37–39. The shock transmits the interface perfectly, independently of its strength.

Hence for strongly dissipative schemes and a fixed shock speed, the transmission does not depend on the strength of the shock.

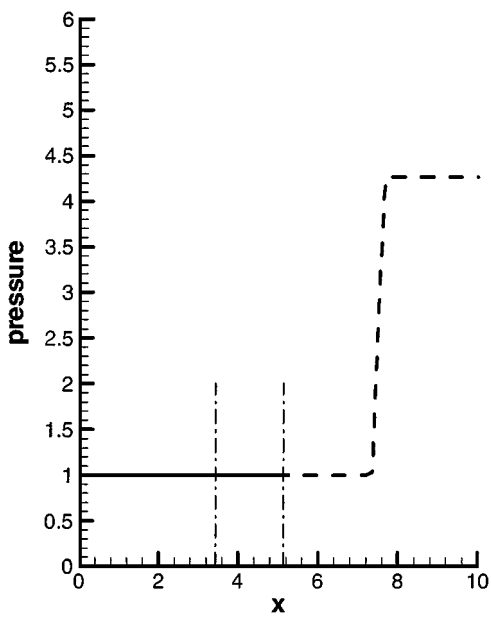

FIG. 42. Computed pressure at instant $t = t_{right}$. van Leer scheme for $M = 2$, $s = 0.05$.

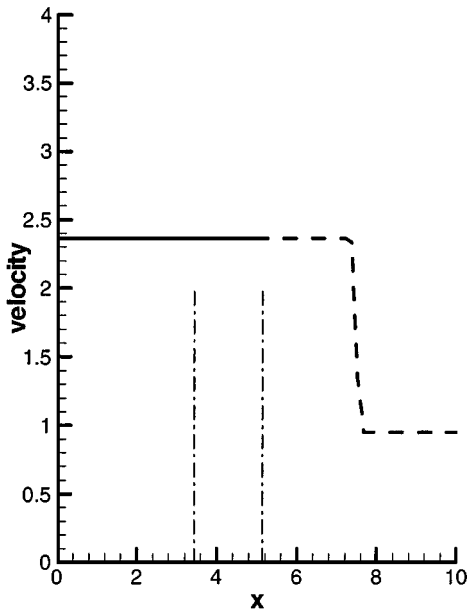

FIG. 43. Computed velocity at instant $t = t_{right}$. van Leer scheme for $M = 2$, $s = 0.05$.

4.5. *Transmission for Different Parts of the Wave*

There are three characteristic speeds for the system of Euler equations. We have only displayed the density in the above numerical tests. One would wonder whether the different characteristic waves have different transmission behaviors. As we have claimed in Section 2.2, no part of the wave is preferred. In order to check this claim, we display other components of the wave. One can choose to display different components, such as the components for the conservative variable, the characteristic variable, or the primitive variable. Since each set of variables can be obtained from a combination of another set of variables it is sufficient enough to display one set of variables. Here we choose to display the primitive variables (ρ, p, u).

We use $M = 2$ and $s = 0.05$. Since the density has already been displayed, here we only display the pressure and velocity. Besides, we only display the results at $t = t_{middle}$.

First we use the Lax–Wendroff scheme for which the shock fails to transmit. The pressure and velocity are displayed in Figs. 40 and 41, respectively. Hence as for the density (Fig. 9), the jumps for both the pressure and the velocity are caught at the interfaces.

Now we use the van Leer scheme for which the shock transmits. The pressure and velocity are displayed in Figs. 42 and 43, respectively. Hence as for the density (Fig. 30), the jumps for both the pressure and the velocity transmit the interfaces.

Hence if the scheme is only weakly dissipative and if the shock is very slow, all the wave components fail to transmit the overlap. If the scheme is sufficiently dissipative, all the components transmit the interface. This means that no part of the wave is preferred.

5. CONCLUDING REMARKS

Based on the previous scalar study and the present system study, we see that the transmission of a moving shock across a grid interface, which is the direct representation of

conservation at a finite mesh size, is controlled by one of the following three factors: (a) shock speed of the exact problem, (b) numerical viscosity of the interior difference equation, and (c) interpolation.

Actually, we observed that if the shock fails to transmit the interface, then a nonphysical, two-shocked steady-state is reached after a long time integration. According to the present study, it is sufficient that only one of these three factors dominates if we want to avoid two-shocked solution. This can be understood through an energy point of view:

(1) if the shock speed is large, then its energy is high enough to overcome energy loss due to nonconservative interpolation;

(2) if the interior difference equation has an enough amount of numerical viscosity, then the perturbation caused by the nonconservative interpolation at the interface can be easily damped out;

(3) if the interpolation is conservative, then no energy is lost at the interface.

For a specific overlapping grid treatment, the three factors exist simultaneously so that the range for the existence of two-shocked solution is very narrow.

Since the dissipation of the interior difference equations helps transmission, a Navier–Stokes solver would have less trouble than the corresponding Euler solver on overlapping grids with regard to conservation.

REFERENCES

1. R. Abgrall, How to prevent pressure oscillations in multicomponent flow calculations: A quasi conservative approach, *J. Comput. Phys.* **125**, 150 (1996).
2. C. B. Allen, The reduction of numerical entropy generated by unsteady shock waves, *Aeronaut. J.* **101**, 9 (1997).
3. M. Arora and P. L. Roe, On postshock oscillations due to shock capturing schemes in unsteady flows, *J. Comput. Phys.* **130**, 25 (1997).
4. R. M. Axel and P. K. Newtown, The interaction of shocks with dispersive waves-II. Incompressible-integrable limit , *Stud. Appl. Math.* **100**, 311 (1998).
5. M. Berger, On conservation at grid interfaces, *SIAM J. Numer. Anal.* **24**, 967 (1987).
6. G. Chesshire and D. Henshaw, Composite overlapping meshes for the solution of partial differential equations, *J. Comput. Phys.* **90**, 1 (1990).
7. G. Chesshire and D. Henshaw, A scheme for conservative interpolation on overlapping grids, *SIAM J. Sci. Comput.* **15**, 819 (1994).
8. B. Engquist and B. Gustafsson, Steady-state computations for wave propagation problems, *Math. Comput.* **49**, 39 (1987).
9. R. P. Fedkiw, T. Aslam, B. Merriman, and S. Osher, A non-oscillatory Eulerian approach to interfaces in multimaterial flows (the Ghost Fluid Method), *J. Comput. Phys.* **152**, 457 (1999).
10. B. Gustafsson, The Euler and Navier–Stokes equations. Wellposedness, stability and composite grids, in *Computational Fluid Dynamics*, von Karman Institute for Fluid Dynamics Lecture Series 1991–2001 (1991).
11. C. Hirsch, *Numerical Computation of Internal and External Flows*, (Wiley, Chichester, 1990), Vols. 1 and 2.
12. S. Jin and J. G. Liu, The effect of numerical viscosities. I. Slowly moving shocks, *J. Comput. Phys.* **126**, 373 (1996).
13. S. Karni, Multi-component flow calculations by a consistent primitive algorithm, *J. Comput. Phys.* **112**, 31 (1994).
14. S. Karni, Hybrid multifluid algorithms, *SIAM J. Sci. Comput.* **17**, 1019 (1996).
15. S. Karni and S. Canic, Computations of slowly moving shocks, *J. Comput. Phys.* **136**, 132 (1997).

16. H.-O. Kreiss and J. Lorenz, *Initial-Boundary Value Problems and the Navier–Stokes Equations*, Academic Press, San Diego, 1989.
17. P. Lax and B. Wendroff, System of conservation laws, *Comm. Pure Appl. Math.* **XIII**, 217 (1960).
18. W. C. Lin, Dissipation additions to flux difference splitting, *J. Comput. Phys.* **117**, 20 (1995).
19. W. C. Lin, Hyperbolic conservation laws with a moving source, *Comm. Pure Appl. Math.* **52**, 1075 (1999).
20. M. S. Liou, A sequel to AUSM: AUSM(+), *J. Comput. Phys.* **129**, 364 (1996).
21. K. R. Meadows, D. A. Caughey, and J. Casper, Computing unsteady shockwaves for aeroacoustic applications, *AIAA J.* **32**, 1360 (1994).
22. F. R. Olsson and N. A. Pertersson, Stability of interpolation on overlapping grids, *Comput. Fluids* **25**, 583 (1996).
23. S. Osher, Riemann solvers, the entropy condition and difference approximations, *SIAM J. Numer. Anal.* **21**, 217 (1984).
24. E. Pärt and B. Sjögreen, *Shock Waves and Overlapping Grids*, Uppsala University, Department of Scientific Computing, Report No. 131, 1991.
25. E. Pärt-Enander and B. Sjögreen, Conservative and non-conservative interpolation between overlapping grids for finite volume solutions of hyperbolic problems, *Comput. Fluids* **23**, 551 (1994).
26. S. V. Parter, On the overlapping grid method for elliptic boundary-value problems, *SIAM J. Numer. Anal.* **36**, 819 (1999).
27. T. W. Roberts, The behavior of flux difference splitting schemes near slowly moving shock waves, *J. Comput. Phys.* **90**, 141 (1990).
28. P. L. Roe, Approximate Riemann solvers: Parameter vector and difference schemes, *J. Comput. Phys.* **43**, 357 (1981).
29. G. Starius, On composite mesh difference methods for hyperbolic differential equations, *Numer. Math.* **35**, 241 (1980).
30. E. Tadmor, Numerical viscosity and the entropy condition for conservative difference schemes, *Math. Comput.* **43**, 369 (1984).
31. H. S. Tang and T. Zhou, On nonconservative algorithms for grid interfaces, *SIAM J. Numer. Anal.* **37**, 173 (1999).
32. M. Thuné, *Stability of Difference Approximations of Hyperbolic Systems on Substructured Domains*, Uppsala University, Department of Scientific Computing, Report No. 106, 1986.
33. Z. J. Wang, A fully conservative interface algorithm for overlapping grids, *J. Comput. Phys.* **122**, 96 (1995).
34. Z. N. Wu, Uniqueness of steady state solutions for difference equations on overlapping grids, *SIAM J. Numer. Anal.* **33**, 1336 (1996).
35. Z. N. Wu, Convergence study of an implicit multidomain method for compressible flow computations, *Comput. Fluids* **25**, 181 (1996).
36. Z. N. Wu, Steady and unsteady shock waves on overlapping grids, *SIAM J. Sci. Comput.* **20**, 1850 (1999).
37. Z. N. Wu and H. Zou, Grid overlapping for implicit parallel computations of compressible flows, *J. Comput. Phys.* **157**, 2 (2000).
38. Z. N. Wu, Slowly moving shock waves for the Euler equations in gas dynamics, submitted for publication.
39. K. Xu and J. S. Hu, Projection dynamics in Godunov-type schemes, *J. Comput. Phys.* **142**, 412 (1998).